Polypyrrole@polyaniline-reduced graphene oxide nanocomposite support material and Cobalt for the enhanced electrocatalytic activity of nickel phosphide microsphere towards alkaline urea oxidation

Materials Research Express

OPEN ACCESS

RECEIVED
29 July 2021

REVISED
26 August 2021

ACCEPTED FOR PUBLICATION
31 August 2021

PUBLISHED
9 September 2021

PAPER

Polypyrrole@polyaniline-reduced graphene oxide nanocomposite support material and Cobalt for the enhanced electrocatalytic activity of nickel phosphide microsphere towards alkaline urea oxidation

Israel Leka Lera[1], **Sutripto Khasnabis**[2], **Lodrick Makokha Wangatia**[1], **Olu Emmanuel Femi**[1,3,*] and **Praveen C Ramamurthy**[2,4,*]

[1] Department of Materials Science and Engineering, Jimma Institute of Technology, Jimma 378, Ethiopia
[2] Indian Institute of Science, Department of Materials Engineering, Bengaluru, Karnataka, India
[3] Mailing address: Faculty of Materials Science and Engineering, Jimma Institute of Technology, Jimma, Ethiopia, PO Box: 378, Jimma University.
[4] Mailing address: Department of Materials Engineering, Indian Institute of Science, Bengaluru-560012 Karnataka, India.
[*] Authors to whom correspondence should be addressed.

E-mail: getuleka22@gmail.com, sutripto.99@gmail.com, lodricksw@yahoo.com, foluemm@gmail.com and praveen@iisc.ac.in

Keywords: current density, electrocatalyst, nickel phosphide, onset potential, urea oxidation, kinetics

Abstract

Efficient and low-cost materials are highly demanded to improve the sluggish kinetics and stability of direct urea fuel cells for large-scale commercialization. In this study, modification of conventional nickel phoaphide (NiP) by cobalt doping via the facile solvothermal method and simultaneously dispersing prepared cobalt nickel phosphide (CoNiP) on poly (aniline-co-pyrrole)/reduced graphene oxide (PPy@PANI/rGO) as efficient and low-cost support material via simple ultrasonic/heat mediated dispersion process. The synthesized catalysts were characterized by scanning electron microscopy and an x-ray diffractometer. Furthermore, Cyclic Voltammetry tests were conducted to evaluate the performance of synthesized catalysis towards alkaline urea oxidation. The physical characterization depicts the successful formation of NiP and Co-doped NiP microsphere with a particle size of 4.306 μm and 2.04 μm, respectively. In addition, homogeneous distribution of the CoNiP microsphere in the structure of PPy@PANI/rGO support material was achieved. Based on the CV test, the superior electrocatalytic performance of CoNiP@PPy@PANI/rGO electrode material with a potential of 0.414V versus SCE to drive a high current density of 26.92 $mAcm^{-2}$, lower onset potential of 0.204 V versus SCE, and higher electrochemically active surface area of 2.08×10^{-1} cm^2mg^{-1} were achieved. Furthermore, the electrochemical activities, kinetics, and stability of CoNiP@PPy@PANI/rGO remarkably outperformed the commercial NiP and CoNiP towards alkaline urea electro-oxidation. Therefore, a novel material, CoNiP@PPy@PANI/rGO, is an excellent candidate for anode electrode material in direct urea fuel cells.

1. Introduction

Technological advancement coupled with fossil fuel depletion, energy crises, and the living standards of society calls for clean, sustainable, and simple energy sources like the supercapacitor, batteries, fuel cells, etc. Among them, a fuel cell such as polymer electrolyte membrane fuel cell, solid oxide fuel cell, direct methanol fuel cell, direct ethanol fuel cell, and direct urea fuel cell, etc. have been attracted tremendous attention of researchers due to their simplicity with minor to no release of toxic pollutants to the environment [1]. Furthermore, direct urea fuel cell (DUFC) has attracted significant attention among fuel cells due to availability, low theoretical potential voltage, high hydrogen content, stability, and inflammability of urea. However, the sluggish kinetics of the anodic reaction and the design and development of highly efficient and low-cost electrode material for the large-

scale commercialization of direct urea fuel cells is a challenging task [2]. So far, noble metals were utilized to enhance the electrochemical performance of direct urea fuel cells [3–5], but their high cost, scarcity, and low CO tolerance limited their wide applications.

Recently, transition metal, particularly Ni-based electrocatalysts like C@NiO [6], NiO@Graphene NC [7], tungsten-doped nickel catalyst (Ni-WOx) [8], graphene supported Ni-NiO Nanoparticles [9], and nickel phosphide [10] were developed by different research groups for enhanced electrochemical oxidation of urea. Among Ni-based transition metal electrocatalysts, nickel phosphide electrode materials have attracted significant research interest due to their anticorrosion properties, superconductivity, magnetic properties, magnetoresistance behavior, and a low bandgap of 1eV, etc. [11–14]. In addition, the delocalized electron distribution in the electronic structure of metal-rich nickel phosphide due to the Ni–Ni metallic bond contributes to the fast kinetics of urea electro-oxidation [14], making it a promising candidate for the urea oxidation reaction. However, the high onset potential, current leakage in long-term cycling, and fast loss of electrochemically active surface area remain challenging.

Recent advancements to enhance the electrochemical performance of nickel phosphide emphasize a simple approach like varying Ni:P molar ratio and heteroatom doping, among others. Lin-Nan *et al* previously suppressed the electrocatalytic activities of NiP for oxygen evolution reaction by using Co as a dopant [15]. Amorim *et al* fabricated Ni electronic structure by doping different molar ratios of Co for oxygen evolution and hydrogen evolution reactions and achieved improved electrocatalytic activities and stability compared with CoP and NiP [16]. Shuai *et al* likewise modified the NiP electronic structure by Co doping and achieved outstanding electrocatalytic activities of CoNiP nanowire towards oxygen evolution and hydrogen evolution reactions [17]. Nevertheless, the lower current density and higher onset potential or overpotential remain a challenge.

Recently, the efforts to improve the electrochemical performance of ternary cobalt-nickel-phosphide electrocatalyst have led to the development of simple approaches like efficient, low-cost, and active support materials. Among the support materials used, graphene has attracted tremendous attention from researchers due to its planarity, high conductivity, high specific surface area, modulus constant, mechanical and chemical stability [18]. Liu *et al* previously suppressed the microhardness, friction reduction, wear resistance, and corrosion resistance of CoNiP using graphene oxide (GO) as a support material [19]. Ye *et al* improved the electrochemical performance of hollow CoNiP in terms of onset potential, over-potential, current density, and durability towards oxygen evolution reaction in alkaline media by using reduced graphene oxide as an efficient support material [18]. However, restacking, exploitation during processing, easy surface corrosion, and agglomeration due to sp^2 hybridized carbon limited its application in electrochemical devices [20, 21]. Thus, incorporating conducting polymers into the structure of reduced graphene oxide as an efficient approach was developed to solve the problems mentioned above [22, 23].

Conducting polymers are conductive materials applied in energy storage and conversion devices as electrode materials or support materials for electro-catalysts. They are flexible, have high corrosion resistance, high conductivity, high redox properties, and conjugated-electronsin theirπ backbone [24, 25]. Among the conducting polymer, polyaniline and polypyrrole have attracted interest due to their high conductivity, chemical stability, redox properties, etc. [26, 27]. Polyaniline and polypyrrole was applied as electrode material in supercapacitors [28], batteries [29], fuel cells [30], light-emitting diode (LED) [31], photocatalysis [32], electromagnetic shielding [33] and sensor [34]. Mousavi *et al* showed that when conducting polyaniline is incorporated into graphene's structure; the resulting nanocomposite can suppress the aforementioned problems of graphene [35]. It was reported that the blends of conducting polymer show enhanced electrical, mechanical, and chemical stability, conductivity, surface area compared with the pristine components due to intermolecular interaction between polymer macromolecules and increased number of sp^2 imine functional group, which is beneficial for energy conversion applications [36]. Usman *et al* incorporated polyaniline-chitosan into the chain of reduced graphene oxide and achieved high thermal stability, conductivity, and lowest bandgap in the ternary composite compared with PANI/rGO [37]. Liang *et al* reported the highest thermal stability and superior electro-catalytic activities of poly (aniline-co-pyrrole) coated reduced graphene oxide compared with PANI/rGO and PPy/rGO as supercapacitor electrode material [38]. Therefore, conducting polymer blend incorporated reduced graphene oxide might be an efficient support material to improve the electrochemical performance of nickel phosphide. Despite many papers that have been reported, this is an area that has received less attention to the best of our knowledge. Therefore, incorporating poly (aniline-co-pyrrole) in reduced graphene oxide chain and using it as an efficient and low-cost support material to improve the electrochemical performance of NiP can be an efficient approach to develop a novel anode electrode material (CoNiP@PPy@PANI/rGO) for alkaline urea electro-oxidation. This is possible because the polymer's conducting layer provides more electrochemically active sites, shortens the path for ions and electron transport resulting from strong interaction between polymer and reduced graphene oxide.

In this study, we synthesized and modified NixP1-x via the combination of facile solvothermal and simple ultrasonic/heat-mediated dispersion process using ferromagnetic Cobalt as dopant and conductive

PPy@PANI/rGO composite as support material. The electrochemical performance CoNiP@PPy@PANI-rGO was compared with NiP, and CoNiP to examine the effect of conductive PPy@PANI/rGO framework. PPy@PANI/rGO supported CoNiP (CoNiP@PPy@PANI/rGO) exhibited a high electrochemical performance due to its high electrochemically active surface area, high kinetics, and stability towards alkaline urea oxidation.

2. Methodology

2.1. Chemicals

Nickel chloride hexahydrate (NiCl2.6H2O, 97%), sodium hypophosphite monohydrate (NaH2PO2.H2O, 98%–101.0%),CoCl2.6H2O, N,N-dimethylformamide (C3H7NO, 99.5%), p-toluene sulfonic acid (C12H18O3S, 98%), aniline hydrochloride (C9H10N4.HCl, 99%), cetyltrimethylammonium bromide (C19H4BrN, 98%), ammonium persulfate ((NH4)2S2O8, 98%), pyrrole (C4H5N, 98%, AR), ethanol (C2H5OH, 99.9%), (L-ascorbic acid (C6H8O6, 99.7), hydrochloric acid (HCl, 37%) and pyrrole (C4H5N, 98%).

2.2. Synthesis of CoNiP

CoNiP was synthesized by using the Solvothermal method reported in the literature with minor modification [30]. Briefly, 0.95 g of $NiCl_2.6H_2O$, 0.143 g of $CoCl_2.6H_2O$, and 0.212 g of $NaH_2PO_2.H_2O$ were taken in 250 ml of a beaker in the molar ratio of Ni:Co:P of 2:1:1. Then 20 ml of DI water was added and ultrasonicated for 30 min. To this mixture, 20 ml of DMF was added and shaken manually for about 5 min. Then this suspension was transferred into stainless steel autoclave and the autoclave was heated at 160 °C for 16 h in a furnace. After 16 h, the mixture was cooled naturally, filtered, washed with DI water and ethanol, and dried at 90 °C for 12 h in a vacuum oven to get CoNiP powder. Then the obtained powder was annealed at 350 °C for 2 h at a heating rate of 2.5 °C min^{-1} to get the final CoNiP powder.

2.3. Synthesis of reduced graphene oxide

GO was synthesized according to the Modified Hummers Method [31]. Reduced graphene oxide was synthesized by reduction of GO using L-ascorbic acid as a reducing agent. Briefly, graphene oxide (1.3 g) was added to 100 ml of water and ultrasonicated for 30 min 5 M L-AA (20 ml) was poured into GO suspension, heated at 60 °C for 12 h, cooled at room temperature, filtered, washed with DI water and ethanol, and dried at 80 °C for 12 h in a vacuum oven.

2.4. Synthesis of PANI@PPy/rGO

PPy@PANI-rGO was prepared by a simple one-pot, two-step, oxidative polymerization method [32]. In this method, 20 ml of p-TSA (20 mmol) was added to 1 g of aniline hydrochloride (ANHC) along with 0.15 g Cetyltrimethylammonium bromide (CTAB) and 10 ml DI water. To the resulting solution, 0.181 g of rGO was added slowly and it was stirred at 0 °C (in an ice bath) for 2 h. Then, a solution of 1 g APS in 10 ml DI water was added to the ANHC/rGO solution very slowly using a dropping funnel (at ~ -5 °C) to carry out the polymerization reaction to form Polyaniline (PANI). After 30 min stirring, the reaction mixture was turned green confirming the formation of PANI. After the green color of the mixture formed, 1 ml of distilled pyrrole was added, and the stirring was continued at 0 °C overnight for the co-polymerization to take place. This mixture was centrifuged and washed with DI water and ethanol (3–4 times) and dried in a vacuum oven at 60 °C for 12 h.

2.5. Synthesis of CoNiP@PPy@PANI-rGO

For the preparation of CoNiP@PPy@PANI-rGO hybrid material, 0.8 g of PANI@PPy-rGO and 200 ml of DI water were taken in 250 ml two necked round bottom flask and stirred for 30 min. To this mixture, 0.15 g of CoNiP was added and stirring was continued overnight at 50 °C. Then cooled down at room temperature, filtered, washed with DI water and ethanol, and dried in a vacuum oven at 80 °C for 12 h.

2.6. Characterization

The crystallinity and phases of synthesized catalyst materials were characterized by x-ray Diffraction (Rigaku x-ray Diffractometer) by using Cu Kα radiation ($\lambda = 1.540598$ Å) in scattering range (2θ) of 5°–80°. The morphological structure of materials was evaluated by High-resolution FESEM (Carl Zeiss).

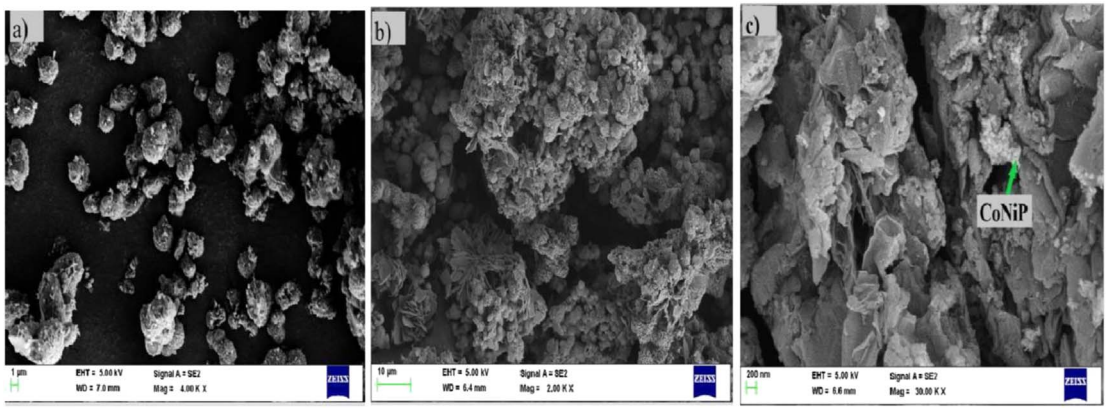

Figure 1. SEM images of (a) NiP (b) CoNiP and (c) CoNiP@PPy@PANI-rGO.

2.7. Electrochemical study

2.7.1. Ink preparation

For ink preparation, 10 mg of sample was used into which 20 μl of Nafion and 1000 μl of ethanol were added. The mixture was ultrasonicated for 15 min to get a homogeneous solution as ink.

2.7.2. Preparation of working electrode

To prepare the working electrode, a glassy carbon electrode was polished using aluminum oxide powder until a shiny surface was obtained. Then it was ultrasonicated for about 10 min in DI water to remove aluminum oxide particles from the electrode surface, rinsed with DI water, and dried at room temperature. After the electrode was dried, 20 μl of ink was doped on the surface of the electrode. Then ink on the electrode was dried overnight at room temperature to get the working electrode.

2.7.3. Electrochemical measurement

The electrocatalytic activities of as-synthesized hybrid materials were tested by using cyclic voltammetry. Three electrode system was used in which sample coated glassy carbon was used as working electrode, platinum wire as reference electrode, and standard calomel electrode (3 M KCl(aq)) as the counter electrode. Nitrogen saturated 5 M KOH with and without 0.33 M urea was used as an electrolyte solution. 30 CV cycle in a potential range of -0.02 to 0.7 V at a scan rate of 0.02 Vs^{-1} in 5 M KOH was recorded to activate the electrode surface before the experiment.

3. Result and discussion

3.1. Microstructure morphologies and equilibrium phases

In this study, the efficiency of the as-synthesized CoNiP@PPy@PANI-rGO electrode material and NiP and Co-doped NiP were compared to determine the effect of the incorporated support material towards urea oxidation in alkaline media. The morphology of the as-synthesized materials was evaluated using scanning electron microscopy (figures 1(a)–(c)). As shown in figure 1(a), a spherical NiP particle with an average particle size of 4.306 μm was achieved. After Co doping, a mixture of spherical and crumpled foil-like morphology of CoNiP in the forms of irregularly stacked petals of a flower was observed [39–41] (figure 1(b)). The morphological changes of NiP after the dispersion of Cobalt reveals the successful deposition of Co in the electronic structure of NiP [17, 42]. The presence of Co in the nickel phosphide structure is also confirmed by the ICP-MS (Inductively coupled plasma-mass spectroscopy), showing the estimated weight percentage of cobalt and nickel elements present in the NiP, CoNiP, and CoNiP@PPy@PANI-rGO (table 1). This change of morphology can be due to the change in geometrical symmetry or the binding environment of the Ni-P electronic structure. As seen from figure1(c), the spherical CoNiP randomly dispersed on the surface of the blend and layered structure of poly (aniline-co-pyrrole)-reduced graphene oxide support material. It is believed that rGO acts as an electron acceptor and aniline and pyrrole act as electron donors, thus forming a weak charge-transfer complex. Therefore, these monomers adsorbed onto the surface of reduced graphene oxide sheets due to electrostatic attraction. The reduced graphene oxide provides a large number of active sites for the nucleation of monomers [43]. The overall coverage of grown monomer on the surface of reduced graphene oxide, the layered structure at the edge of nanocomposite could not be observed. The highly interconnected chain of polyaniline@polypyrrole-

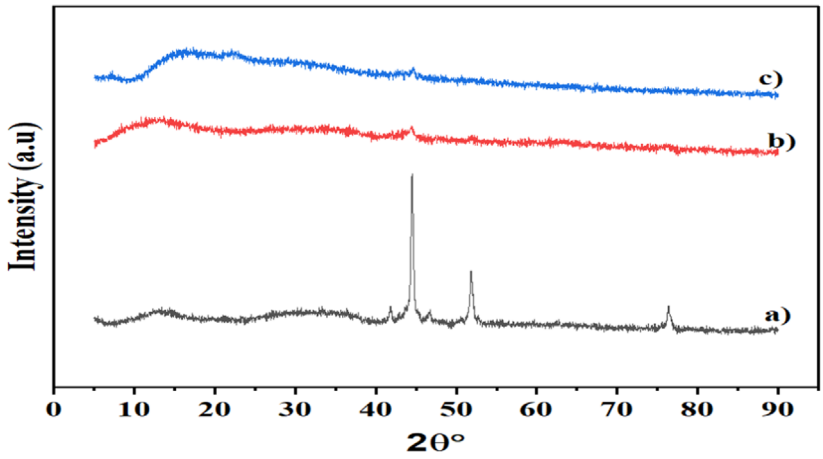

Figure 2. XRD patterns of (a) NiP (b) CoNiP and (c) CoNiP/PPy@PANI-rGO.

Table 1. ICP-MS results indicating the concentration of Co and Ni elements present in NiP, CoNiP, and CoNiP@PPy@PANI-rGO.

Catalysts		Ni		Co
	Conc. [PPb]	Conc. [RSD]	Conc. [PPb]	Conc. [RSD]
NiP	0.068	14.018	NA	NA
CoNiP	0.064	8.78	0.814	3.030
CoNiP@PPy@PANI-rGO	0.177	2.52	0.163	3.540

NA = Not assigned

reduced graphene oxide provides a high surface area and high conductivity, which is favorable for enhanced electrochemically active surface area, dispersion of CoNiP nanoparticles, and high charge transport of the composite.

The crystal structure and phase of the as-synthesized hybrid materials were characterized by an x-ray diffractometer. As seen from figure 2(a), the diffraction peak at $2\theta = 41.8°$ corresponding to Ni12P5 phase (JCPDS No. 65-1623), the diffraction pattern at $2\theta = 44.6°$ (201) exhibits Ni2P crystalline phase of nickel phosphide (JCPDS, No. 03-0953). The peak centered at $2\theta = 46.6°$ corresponding to Ni3P crystalline phase (PDF card 65-1605), the diffraction pattern centered at $2\theta = 51.7°$ (200) corresponding to cubic Ni phase (JCPDS No. 04-0850). This result indicates the mixture of Ni2P, Ni12P5, Ni3P, and Ni cubic crystallographic phases and amorphous phase at around $2\theta = -3213.7°$. The experimental conditions like heat treatment and the used atmosphere influences the formation of different crystallographic nickel phosphide phases. For example, heat treatment at a lower concentration of phosphorus precursor results in the mixture of Ni3P, Ni12P5, and NiP and two overlapping phases like Ni12P5/Ni2P and a small amount of impurities like NiCl (H2PO2)(H2O) due to incomplete chemical reactions between nickel precursor and phosphorus sources [44]. In solvothermal reaction, sodium hypophosphite (NaH2PO2.H2O) releases PH3 gas upon decomposition at a higher temperature. The generated PH_3 diffuses onto the nickel surface and subsequently reduces Ni^{2+} to form nickel phosphide. However, an insufficient amount of PH3 results in a disproportionation reaction that produces other crystallographic phases like Ni12P5, NiP, Ni3P, and Ni, hence Ni cubic crystallographic phases in our sample. As seen from figures 2(b) and (c), the main diffraction centered at $2\theta = 44°$ (201) corresponding to the crystallographic phases of Ni2P (JCPDS, No. 03-0953) was observed. Upon addition of Co, the peak intensity decreased, indicating that Cobalt affected the crystal structure of Ni-P particles [42]. The other diffraction peaks gradually disappeared, indicating the interaction of the NiP terminal phase with cobalt nanoparticles through metallic and ionic bonds and polymer-graphene chain, imine nitrogen and via electrostatic interaction [42].

The sharp and interaction intensive peak exhibits the high crystallinity of NiP catalyst. The increased amorphousness of Co and poly(aniline-co-pyrrole)-reduced graphene oxide incorporated NiP was observed due to electron density regulation or rearrangement. In our study, the Ni content of the as-synthesized samples was measured using ICP-MS. The result reveals very close Ni content in all three synthesized samples, i.e., 0.068, 0.64, and 0.17 for NiP, CoNiP, and CoNiP@PPy@PANI-rGO, respectively, exhibiting no significant loss of Ni during solvothermal method followed by heat mediated dispersion process.

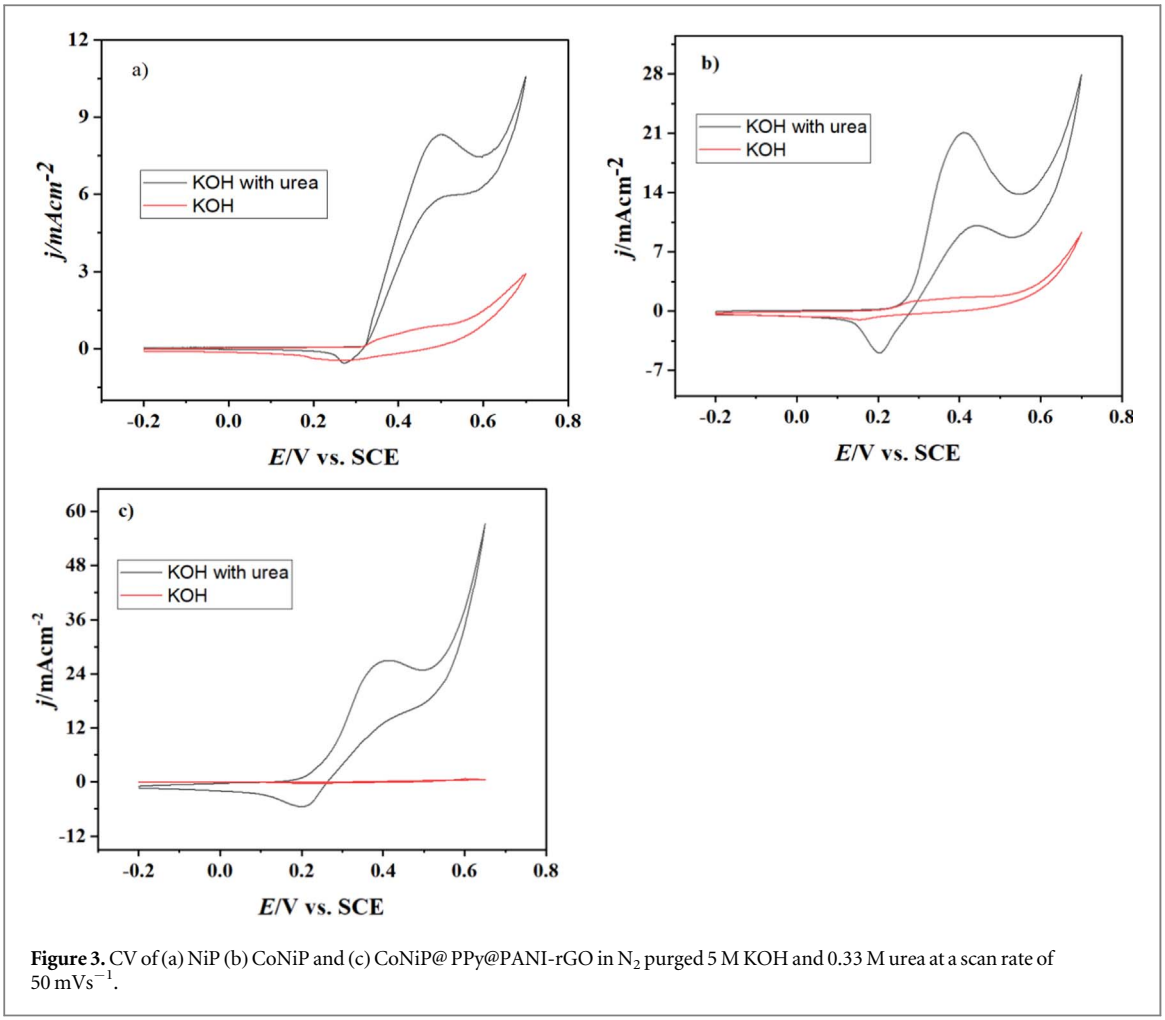

Figure 3. CV of (a) NiP (b) CoNiP and (c) CoNiP@ PPy@PANI-rGO in N_2 purged 5 M KOH and 0.33 M urea at a scan rate of 50 mVs^{-1}.

The catalyst's average crystallite size (t) was computed using the Debye–Scherrer equation, as shown in equation (1) [43].

$$t = \frac{k\lambda}{\beta \cos\theta} \tag{1}$$

t is the crystalline size, k is the constant (0.9), $\beta$is the full width half maximum (FWHM), $\theta$is Bragg's angle in radians, λ is the wavelength (0.15406 nm). The calculated value of crystal size of NiP, CoNiP, and CoNiP@PPy@PANI-rGO was 0.182 nm, 0.176 nm, and 0.01 nm, respectively. This result reveals the decreased crystallite size and interplanar distance of catalyst nanoparticles upon dispersion on the surface of the support material. This can be the increased distribution of nanoparticles on the surface of support materials due to higher active surface area and strong particle interaction with the active site of support material.

3.2. Electrochemical behavior

The electrocatalytic activities of as-synthesized catalysts were studied by cyclic voltameter within a potential range from −0.02 to 0.7 V at a scan rate of 0.05 Vs^{-1} under N2 purged 5 M KOH with and without 0.33 M urea at room temperature. As can be seen from figures 3(a)–(c), A couple of peak potentials centered at 0.492/0.273 V, 0.32/0.163 V, and 0.355/0.205 to derive anodic peak current density of 8.3 $\times$ 10^{-4} $mAcm^{-2}$, 0.09 $mAcm^{-2,}$ and 10.7 $mAcm^{-2}$ for NiP, CoNiP, and CoNiP@PPy@PANI-rGO, respectively was computed in KOH oxidation that reveals the significant efficiency improvement of NiP upon Co doping, and PPy@PANI-rGO used as a support material. Only one oxidation peak current density was observed in KOH solution, indicating no regeneration of blocked Ni active site for oxidation of urea molecules and reaction intermediates during a backward scan. The NiO expands with applied potential and time because of OH^- penetration into its structure and NiO converted -intoandanhydrhydrous-Ni(OH)β2.Withα further increasing potential, anhydrous-Ni (OH)β2 is converted β-NiOOH,into which stable is further converted into γ-NiOOH then the current density decreases [44].

Upon adding urea into KOH solution, the enhancement of anodic current density above the potential of 0.325 V, 0.235 V, and 0.193 V for NiP, CoNiP, and CoNiP@PPy@PANI-rGO, respectively exhibit the higher

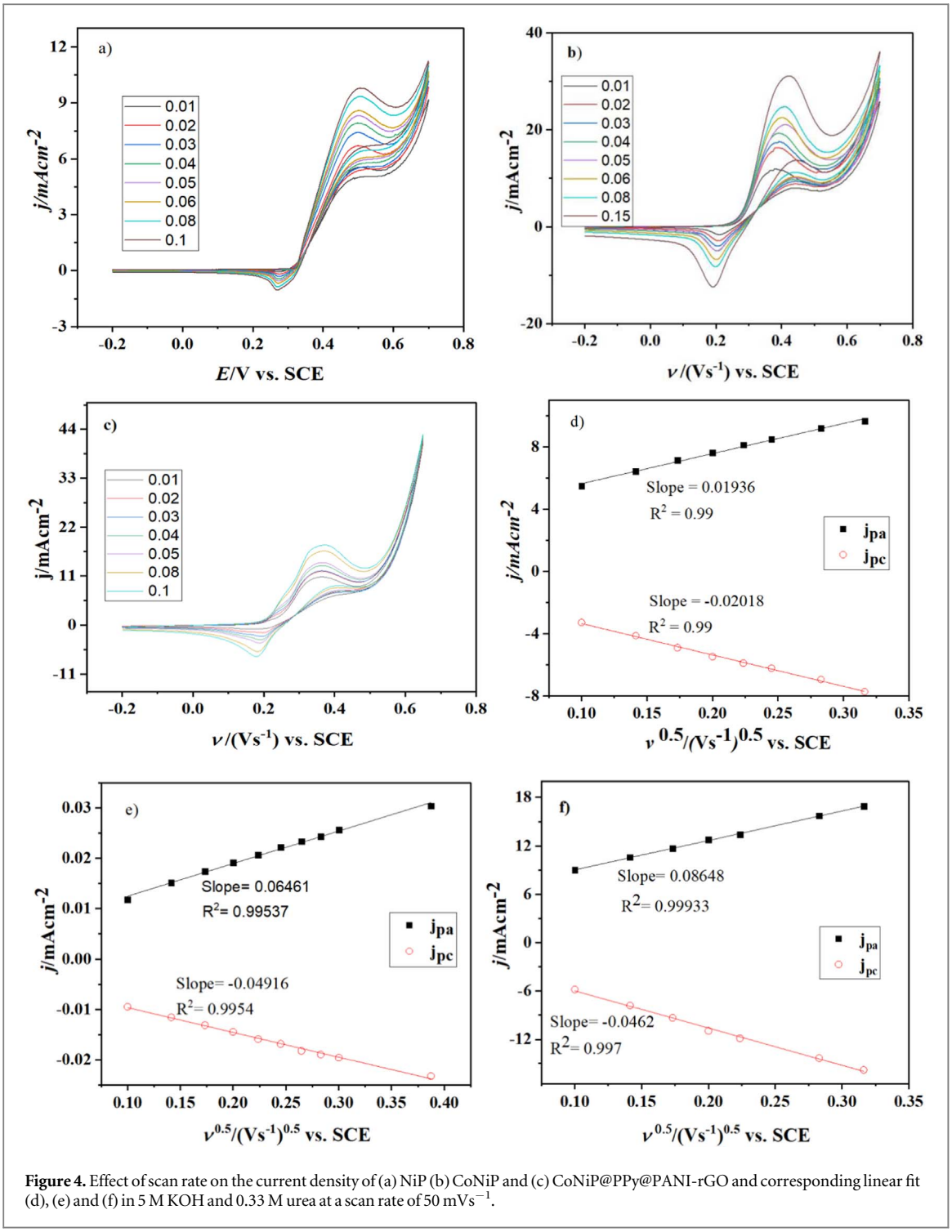

Figure 4. Effect of scan rate on the current density of (a) NiP (b) CoNiP and (c) CoNiP@PPy@PANI-rGO and corresponding linear fit (d), (e) and (f) in 5 M KOH and 0.33 M urea at a scan rate of 50 mVs^{-1}.

electrochemical performance of catalysts towards urea electrooxidation. The anodic current density of 8.32 $mAcm^{-2}$, 21.1 $mAcm^{-2}$, and 26.91 $mAcm^{-2}$ was achieved after urea addition for NiP, CoNiP, and CoNiP@PPy@PANI-rGO at an anodic peak potential of 0.501 V, 0.412 V and 0.41 V, respectively. The oxygen evolution reaction started above the potential of 0.613 V, 0.546 V, and 0.498 V for NiP, CoNiP, and CoNiP@PPy@PANI-rGO, respectively, to the absorption of urea molecules on the surface of NiOOH than OH^- ions. Interestingly another anodic current density at a given potential was observed during the backward scan due to the oxidation of urea molecules and the reaction intermediates after the regeneration of previously blocked N^{+2}/Ni^{+3} active sites. However, the current density recorded during the backward CV scan was lower than the forward scan. This could be incomplete regeneration of Ni's active site for complete oxidation of urea molecules or reaction intermediates. The higher current density and lower onset potential of both Co-doped and poly(aniline-co-pyrrole)/rGO supported CoNiP reveals the reduced electron or charge path and increased conductivity on composite. From this result, the doping of Cobalt and simultaneously decorating with polymer-

rGO support material were good techniques to enhance the electrocatalytic activities of commercial NiP microsphere towards alkaline urea oxidation. These enhancements were related to the synergetic effect of Cobalt [45] and higher electrochemically active surface area, conductivity, and interlinkages of support chains for the homogeneous distribution of NiP particles [46, 47].

Moreover, the incorporation of the Co atom rearranges the electronic structure of Ni and forming a CoOOH and NiOOH active site in the composite. Co doping formed homogeneous mixtures of Ni2P, CoP, and CoNiP crystallographic phases in the CoNiP composite structure [15]. For example, CoP and Ni2P were formed in CNTs@NiCoP/C, NiCoP/C, and Ni2P–CoP and NiCo2Px composite [15]. Therefore, the contribution of an active site from both CoP/CoOOH and Ni2P/NiOOH made the CoNiP catalyst remarkably outperformed towards the urea electrooxidation in alkaline media. Further enhanced electrochemical performance of PPy@PANI-rGO supported CoNiP results from their unique structure, intrinsic electrochemical properties, high charge migration, higher conductivity, and low internal resistance and synergetic effect between PPy, PANI, and rGO [48, 49]. Conducting polymer on the surface of reduced graphene oxide provides large active sites for electrochemical activities and shortens the electron or charge transfer path due to the strong interaction between polymeric chains and reduced graphene oxide [49]. The presence of rGO affects the transport and conformation of the polymeric chain and further reduces the oxygen functional groups of rGO during the *in situ* chemical polymerization process of aniline and pyrrole. Therefore, Co doping and PPy@PANI-rGO as an efficient and low-cost support material for NiP significantly improved the electrochemical performance of nickel phosphide towards alkaline urea electro-oxidation.

The increasing current density during a forward scan and the decrease of current density during a backward scan was a special behavior of the electrochemical regeneration effect (EC' mechanism).

$$OH^- + Ni(OH)_2 \rightarrow H_2O + NiOOH + e^- \quad (2)$$

$$CO(NH_2)2 + NiOOH \rightarrow Ni(OH)_2 + products \quad (3)$$

During electrooxidation of urea, N_2, CO_2, and H_2O were formed in anode whereas H_2 gas was accumulated in cathode as fuel and electron passing through the external circuit according to the following equation:

Anode

$$Ni(OH)_2 + OH^- \rightarrow H_2O + NiOOH + e^- \quad (4)$$

$$e^- + CO(NH_2)2 \rightarrow 5H_2O + N_2 + CO_2 \quad (5)$$

Cathode

$$6H_2O + 6e^- \rightarrow 6OH^- + 3H_2 \quad (6)$$

Overall reaction

$$CO(NH_2)2 + H_2O \rightarrow CO_2 + N_2 + 3H_2 \quad (7)$$

3.3. Effect of scan rate

The effect of scan rate on the electrocatalytic activities of the as-synthesized catalysts was examined towards alkaline urea oxidation at different scan rates. As seen from figures 4(a)–(c), as the scan rate increases, the current density of the system increases due to increased flow of current to compensate for a short time of charge or electron transfer. The shifting of cathodic peak potential to negative potential and anodic peak potential to positive potential was observed, indicating the redox reaction was quis-reversible in three synthesized catalysts. The square root of scan rate versus current density of the system was plotted to determine whether the reaction was diffusion controlled or mixed kinetics. As seen from figures 4(d)–(f), linear relationships between the current density and square root of scan rate reveal the redox reaction was diffusion controlled in urea electro-oxidation in alkaline media.

3.4. Kinetic study

The electron transfer coefficient (αs) and electron transfer rate constant (ks) were computed from the following formula [43]:

$$E_{pa} = E^o + \frac{RT}{(1-\alpha_s)} \ln(1-\alpha_s\left(\frac{nvF}{RTk_s}\right) \quad (8)$$

$$E_{pc} = E^o + \frac{RT}{nF(1-\alpha_s)} \ln\left(\frac{\alpha_s nvF}{RTk_s}\right) \quad (9)$$

$$\ln k_s = \alpha_s \ln(1-\alpha_s) + (1-\alpha_s)\ln\alpha_s - \alpha_s\frac{nF\Delta E_p}{RT} - \ln\left(\frac{RT}{nvF}\right) \quad (10)$$

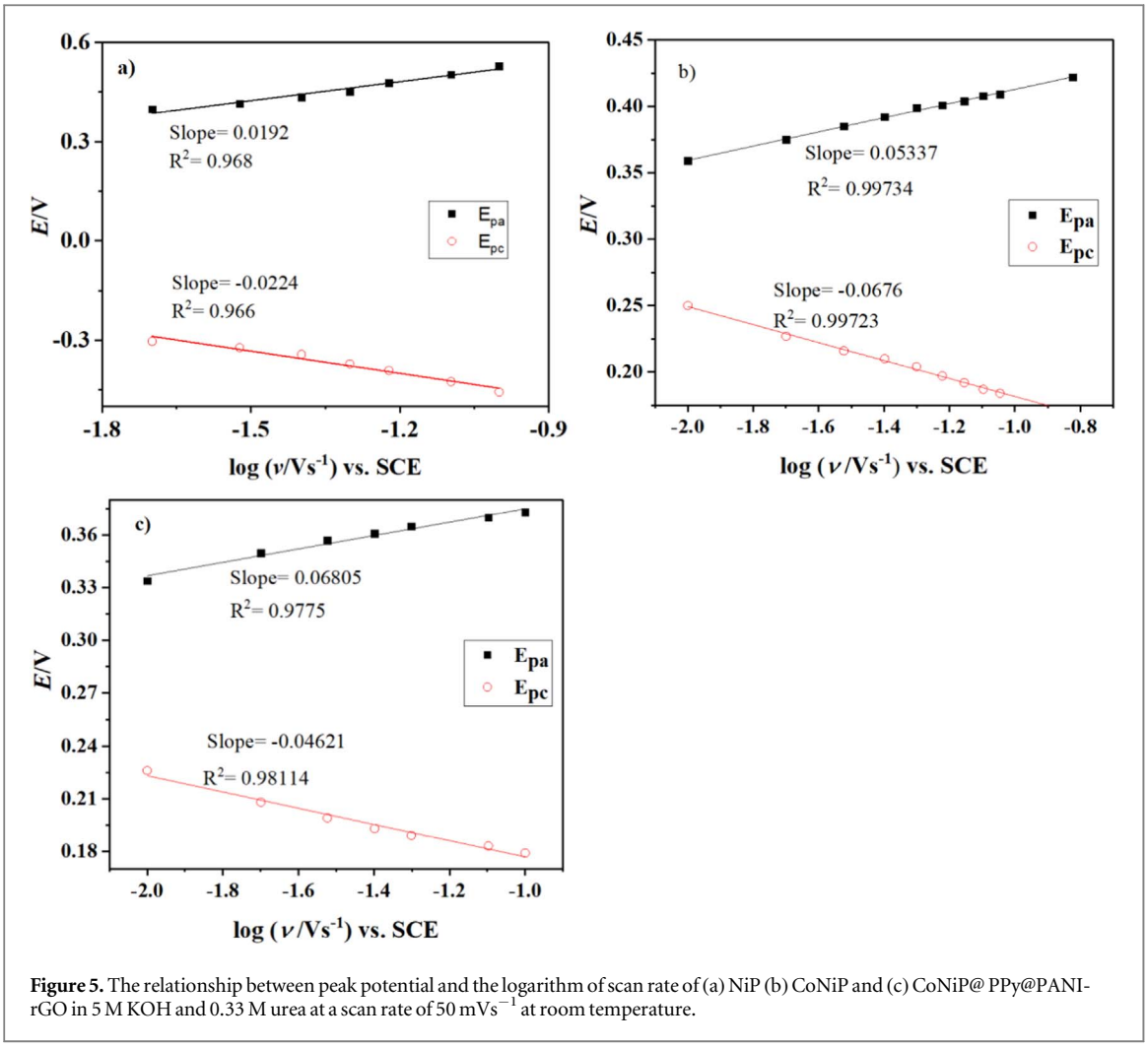

Figure 5. The relationship between peak potential and the logarithm of scan rate of (a) NiP (b) CoNiP and (c) CoNiP@ PPy@PANI-rGO in 5 M KOH and 0.33 M urea at a scan rate of 50 mVs^{-1} at room temperature.

$E°$ is the standard electrode potential, R is the universal gas constant, F is the Faradays constant, T is the absolute temperature, n is the number of electrons transferred, υ is the scan rate, α_s is the electron transfer coefficient determined from the slop of peak potential versus logarithm of scan rate (figures 5(a)–(c)), E_{pa} and E_{pc} are the anodic and cathodic peak potential, respectively. Now the calculated value of α and k_s for NiP, CoNiP and CoNiP@PPy@PANI-rGO is (0.46 and 1.6 $\times$ 10^{-6} s^{-1}), (0.57 and 1.37 $\times$ 10^{-7} s^{-1}), (0.65 and 2.5 $\times$ 10^{-7} s^{-1}), respectively. The electron transfer coefficient value confirms the reaction was diffusion controlled. From the literature, the electron transfer coefficient approaches 0.5 represent the reaction was diffusion controlled whereas 1 exhibit the redox reaction was adsorption controlled [41]. The diffusion coefficient is another important parameter used to determine the degree of ions diffused from higher concentration to lower concentration. The diffusion of ions on electrode surface or interlayer from bulk solution was calculated according to the following Randles-Sevcik equation [42].

$$i_p = 2.99\ x\ 10^5 n[(1-\alpha)n_o]^{\frac{1}{2}} CAD^{\frac{1}{2}}\nu^{\frac{1}{2}} \quad (11)$$

where i_p is the peak current density, n is the total number of electrons transferred in urea oxidation (6), n_o in the number of electrons in rate-determining step (1), C is the concentration of urea [mol/cm^3], A is the geometrical area of the electrode (cm^2), D is the diffusion coefficient (cm^2s^{-1}) and ν is the scan rate (Vs^{-1}). α is the electron transfer coefficient determined from the slope of peak potential (E_p) versus logarithm of scan rate ($\log \nu$) (figures 4(a)–(c)) as [41]: $\frac{S_a}{|-S_c|} = \frac{\alpha}{1-\alpha}$, where S_a is the anodic slope and S_c is the cathodic slope. Then substituting the value of α (0.46, 0.57 and 0.65) for NiP, CoNiP, and CoNiP@PPy@PANI-rGO, respectively) in to equ. 14, the diffusion coefficient of redox reaction in urea oxidation by NiP, CoNiP, and CoNiP@PPy@PANI-rGO electrocatalysts were 0.98 $cm^2\ s^{-1}$, 1.76 $cm^2\ s^{-1,}$ and 2.12 $cm^2\ s^{-1}$. The higher diffusion coefficient and electron transfer rate of poly(aniline-co-pyrrole)/rGO supported CoNiP catalyst is due to the number of the imine nitrogen atom and delocalized π-electrons from support chains that reduce the electron or charge transfer path in urea oxidation reaction which further enhances the electrocatalytic activities of the substrate.

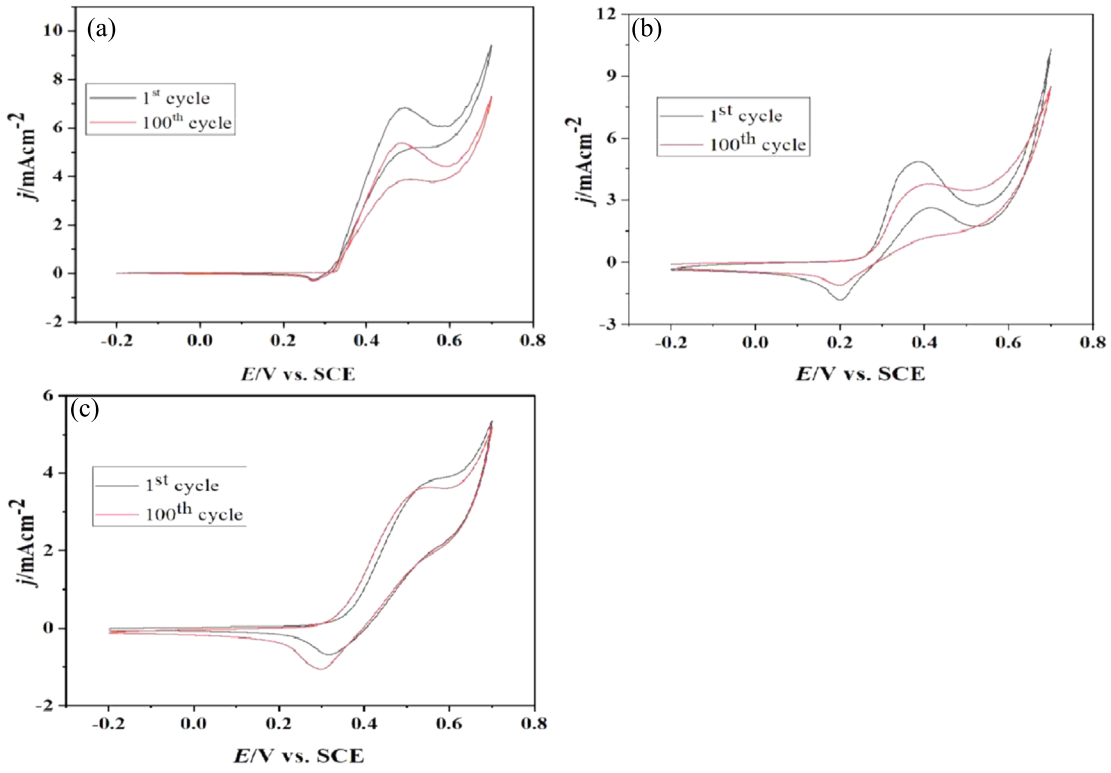

Figure 6. CV graphs of 1st and 50th cycle of (a) NiP (b) CoNiP and (c) CoNiP@PPy@PANI-rGO 1 M KOH and 0.33 M urea at a scan rate of 50mVs^{-1}.

The estimation of electrochemically active surface area was crucial to understanding the electrochemical performance of synthesized catalysts deeply. The electrochemically active surface area was quantified by the integration of charge associated with reduction peak (Q) (Ni^{+3}/Ni^{+2}) in cyclic voltammogram according to the following equation [10]:

$$ECASA = \frac{Q}{[m] * 0.257\ \text{mCcm}^{-2}} \tag{12}$$

Where Q is the integral of an area determined from the reduction peak, m is the mass of catalyst loaded on the electrode surface, 0.257 mCcm^{-2} is the charge associated with the monolayer of Ni^{3+}. Based on this equation, the calculated ECASA value of NiP, CoNiP and CoNiP@PPy@PANI-rGO was 1.28 $\times$ 10^{-1} cm^2 mg^{-1}, 1.47 $\times$ 10^{-1} cm^2 mg^{-1} and 2.08 $\times$ 10^{-1} cm^{2}mg^{-1} respectively. This result indicates the higher electrochemically active surface area of both Co-doped and copolymer-rGO supported CoNiP due to higher active surface area of polymer/graphene chain and the synergetic effect [45, 50].

3.5. Stability test

The stability of as-synthesized catalysts has was evaluated by determining the loss of current density during the 100th of the potential cycle under N2 purged alkaline urea electrooxidation reaction at room temperature. This 100th of the potential cycle was conducted after all CV measurements like the effect of scan rate measurement, electrochemically active surface area measurement, etc. The reduced anodic current density or loss after the 100th CV scan for CoNiP, CoNiP/PPy@PANI-rGO, and NiP computed to be 1.43 mAcm^{-2}, 1.07 mAcm^{-2} and 0.21 mAcm^{-2} respectively (figures 6(a)–(c)). These losses or leakage of current density can be related to the loss of electrochemically active surface area due to dissolution, grain growth, redeposition, coagulation or coalescence, precipitation of catalyst particles, and poisoning of the electrode surface by the reaction intermediates formed during long potential cycling [51–53]. As seen from the current loss value, the doping of Co and simultaneously dispersing the obtained CoNiP on PPy@PANI-rGO conductive film matrix results in an unmeasurable or insignificant loss of current density during the 100th potential cycle indicating the enhanced or improved stability of catalysts. This can be explained by the anticorrosion properties of conducting polymer films together with the chemical stability, high specific surface area, and huge conductivity of rGO interlinked chain that inhibits the electrode surface poisoning intermediates like CO and prevents early dissolution and agglomeration of nanoparticles. Therefore, NiP stability was significantly improved after doping of Cobalt and simultaneous dispersion of CoNiP on the surface of PPy@PANI-rGO support material due to the synergetic effect [16].

4. Conclusion

In summary, synthesis and modification of NiP electronic structure using Co as a dopant and PPy@PANI-rGO as an efficient and low-cost support material was successfully achieved using a facile solvothermal method and ultrasonic/heat-mediated dispersion techniques. The morphological phenomena and crystalline phases of as-synthesized catalysts were characterized using FESEM and XRD techniques. After physical characterization, cyclic voltammetry techniques were used to determine the electrocatalytic activities of as-synthesized catalysts materials towards alkaline urea oxidation. The physical characterization of as-synthesized catalysts indicates the successful formation of microspherical NiP and CoNiP with a particle size of 4.306 μm and 2.04 μm, respectively, and also shows the distribution of CoNiP on PPy@PANI-rGO support material. Based on the CV test, Co doping and supporting the obtained CoNiP using PPy@PANI-rGO showed superior performance compared with conventional NiP. Among the prepared electrode material, CoNiP@PPy@PANI-rGO shows a higher current density of 26.92 $mAcm^{-2}$, lower onset potential of 0.204 V, and high electrochemically active surface area, enhanced kinetics, and high stability compared with NiP and CoNiP. Hence, a novel electrode material CoNiP@PPy@PANI-rGO remarkably outperformed the commercially available NiP and prepared CoNiP, making it a promising candidate as anode electrocatalyst material for alkaline urea oxidation in a direct urea fuel cell.

Acknowledgments

Financial support from the Ministry of science and higher education, Ethiopia. The support from Mr Varun Adiga, Ms Shweta Shekar, Mr Sandeep Satyanarayana, and Dr Simranjeet Singh, Department of Materials Engineering, Indian Institute of Science, was highly acknowledged. Part of this work was conducted at Jimma University, Institute of Technology.

Data availability statement

The data that support the findings of this study are available upon reasonable request from the authors.

Declarations

Funding sources

This work was supported by the Ministry of Science and Higher Education, Ethiopia, and IoE grant R(VI)090/23/2019-20 356 (Indian Institute of Science, India).

Conflicts of interest/Competing interests

The authors declare that they have no known competing financial interests or personal relationships that could have appeared to influence the work reported in this paper

Authors' contributions

Israel Leka: conceptualization, methodology, investigation, writing-original draft, writing-review and editing, validation, project administration Sutripto Khanshi: resources, validation, editing, facilitating Lodrick Wangatia: data curation, supervision, project administration, Femi Olu: data curation, supervision Praveen C Ramamurthy: supervision, validation, Resources, material funding acquisition

Ethics approval-no ethics problem

Consent to participate- participate at all processes

Consent for publication-participate at all processes.

ORCID iDs

Israel Leka Lera https://orcid.org/0000-0001-7501-6304
Olu Emmanuel Femi https://orcid.org/0000-0002-6069-7968

References

[1] Enas Taha *et al* 2017 *Journal of Power Sources* **417** 159–75
[2] Yu B, Feng L, He Y, Yang L and Xun Y 2021 *J. Hazard. Mater.* **401** 123394
[3] Fei L, Sun H, Ran R, Zhou W and Shao Z 2021 *Ind. Eng. Chem. Res.* **60** 1185–93
[4] Ren X, Lv Q, Liu L, Liu B, Wang Y, Liu A and Wu G 2019 *Sustain. Energy Fuels* **4** 15–30
[5] Ramli Z A C and Kamarudin S K 2018 *ChemSusChem* **13** 3357–75
[6] Lu S, Hummel M, Gu Z and Wang Y 2021 *J. Mater.Chem. A* **6** 23220–43
[7] Lu S, Hummel M, Kang S, Pathak R, He W, Qi X and Gu Z 2021 *J. Mater.Sci. Mater. Electron.* **27** 3619–27
[8] Ray A, Sultana S, Paramanik L and Parida KM 2021 *J. Mater.Chem. A* **8** 19196–245
[9] Shuli Wang P X and Jingqi Tian Z L L F 2021 *Electrochim. Acta* **370** 137755
[10] Ding R, Li X, Shi W, Xu Q, Wang L, Jiang H, Yang Z and Liu E 2016 *Electrochim. Acta* **222** 455–62
[11] Weng C C, Ren J T and Yuan Z Y 2020 *ChemSusChem* **13** 3357–75
[12] Pei Y, Cheng Y, Chen J, Smith W, Dong P, Ajayan P M, Ye M and Shen J 2018 *J. Mater. Chem. A* **6** 23220–43
[13] Salavati-niasari A S M 2016 *J. Mater. Sci. Mater. Electron.* **27** 3619–27
[14] Ray A, Sultana S, Paramanik L and Parida K M 2020 *J. Mater. Chem. A* **8** 19196–245
[15] Zhou L N, Yu L, Liu C and Li Y J 2020 *RSC Adv.* **10** 39909–15
[16] Amorim I, Xu J, Zhang N, Xiong D, Thalluri S M, Thomas R, Sousa J P S, Araújo A, Li H and Liu L 2020 *Catal. Today* **358** 196–202
[17] Shuai C, Mo Z, Niu X, Zhao P and Dong Q 2020 *J. Alloys Compd.* **847** 156514
[18] Ye L and Wen Z 2017 *Electrochem. Commun.* **83** 85–9
[19] Liu C, Wei D, Huang X, Mai Y, Zhang L and Jie X 2019 *J. Mater. Res.* **34** 1726–33
[20] Rabl H, Weilend D, Tekoglu S, Seelajaroen H, Neugebauer H, Heitzman N, Apaydin DH, Scharber MC and Sariciftci NS 2014 *J Biofertilizers Biopestic.* **3** 10611–8
[21] Zhankun J and Jeimei YTH 2009 *Technology* **10** 743–53
[22] Sha R, Komori K and Badhulika S 2017 *Electrochim. Acta* **233** 44–51
[23] Sha C, Lu B, Mao H, Cheng J, Pan X, Lu J and Ye Z 2016 *Carbon N. Y.* **99** 26–34
[24] Fan X, Nie W, Tsai H, Wang N, Huang H, Cheng Y, Wen R, Ma L, Yan F and Xia Y 2019 *Adv Sci.* **4** 100047
[25] Dakshayini B S, Raghava K, Mishra A, Shetti N P, Malode S J, Basu S, Naveen S and Raghu A V 2019 *Microchem. J.* **147** 7–24
[26] Rabl H, Wielend D, Tekoglu S, Seelajaroen H, Neugebauer H, Heitzmann N, Apaydin D H, Scharber M C and Sariciftci N S 2020 *ACS Appl. Energy Mater.* **3** 10611–8
[27] Mousavi MF, Hashemi M, Rahmanifar MS and Noori A 2017 *Electrochim. Acta* **228** 290–8
[28] Tikish TA, Kumar A and Kim JY 2018 *Adv MaterSci Eng* **7** 28–33
[29] Usman F, Dennis JO, Seong KC, Yousif AA, Meriaudeau F, Ayodele OB, Tobi AR and Rabih AAS 2021 *Chem Pap.* **15** 102690
[30] Wang H, Lin J and Shen Z X 2016 *J. Sci. Adv. Mater. Devices* **1** 225–55
[31] Ates M, Karazehir T and Sarac A S 2012 *Electrochim. Acta* **222** 455–62
[32] Kumar R, Travas-Sejdic J and Padhye L P 2020 *Chem. Eng. J. Adv.* **4** 100047
[33] Yavuz Ö, Ram M K, Aldissi M, Poddar P and Srikanth H 2005 *Synth. Met.* **151** 211–7
[34] Ramanavičius A, Ramanavičiene A and Malinauskas A 2006 *Electrochim. Acta* **51** 6025–37
[35] Mousavi M F, Hashemi M, Rahmanifar M S and Noori A 2017 *Electrochim. Acta* **228** 290–8
[36] Tikish T A, Kumar A and Kim J Y 2018 *Scientific Reports* **2018** 8–13
[37] Usman F, Ojur J, Cheng K, Yousif A, Meriaudeau F, Bolarinwa O, Ridwan A, Abdelkarim A, Rabih S and Yar A 2019 *Results Phys.* **15** 102690
[38] Lianga B, Qinab Z, Lia T, Doub Z, Zengb F, Caib Y, Zhuab M and Zhou Z 2015 *Electrochim. Acta* **177** 335–42
[39] Shuai M, Lin J, Wu W, Kuang H, Zhang W, Ling Q, Chen H and Komarneni S 2020 *New J. Chem.* **44** 8796–804
[40] Liu J, Chen P, Deng L, He J, Wang L, Rong L and Lei J 2015 *Sci. Rep.* **5** 1–13
[41] Li J, Liu H, Zhang Y, Li Y, Qi D and Chen Z 2020 *J. Sol-Gel Sci. Technol.* **94** 461–7
[42] Tesfaye R M, Das G, Park B J, Kim J and Yoon H H 2019 *Sci. Rep.* **81** 1–9
[43] El-lateef H M A, Almulhim N F, Alaulamie A A and Saleh M M 2020 *Colloids Surfaces A* **585** 124092
[44] Vedharathinam V and Botte G G 2012 *Electrochim. Acta* **81** 292–300
[45] Liang Z, Qu C, Zhou W, Zhao R, Zhang H and Zhu B 2019 *J. Braz.Chem. Soc.* **19** 720–6
[46] Gedler G, Antunes M and Velasco J I 2015 *J. Mater.Sci. Mater. Electron* **26** 6945–53
[47] Yan H, Tang Y and Long W 2014 *J. Electrochem. Soc* **163** 5256–64
[48] Tran V C, Sahoo S, Hwang J, Nguyen V Q and Shim J 2018 *J. Electroanal. Chem.* **810** 154–60
[49] Liang B, Qin Z, Li T, Dou Z, Zeng F, Cai Y, Zhu M and Zhou Z 2015 *Electrochimica Acta* **177** 335–42
[50] Ullah K, Kim I J, Yang S H and Oh W C 2015 *J. Mater. Sci. Mater. Electron.* **26** 6945–53
[51] Sugawara Y, Yadav A P, Nishikata A and Tsuru T 2011 *J. Electroanal. Chem.* **662** 379–83
[52] Zihrul P, Soc J E, Zihrul P, Hartung I, Kirsch S, Huebner G and Gasteiger H A 2016 *J. Electrochem. Soc.* **163** F492
[53] Steven G R, Urchaga P, Hu J, Lee W, Stumper Jürgen, Rice C and Eikerling M 2014 *Phys. Chem. Chem. Phys.* **3** 2–24